Atmospheric atomic layer deposition of SnO 2 thin films with Tin(II) acetylacetonate and water

Viet Huong Nguyen, Masoud Akbari, Abderrahime Sekkat, Huong T. T. Ta, Joao Resende, Carmen Jiménez, Kevin Musselman, David Muñoz-Rojas

Atmospheric atomic layer deposition of SnO_2 thin films with Tin(II) acetylacetonate and water

Viet Huong Nguyen,[1,] Masoud Akbari,[2] Abderrahime Sekkat,[2] Huong T. T. Ta,[1] Joao Resende,[3] Carmen Jiménez,[2] Kevin P. Musselman,[5] David Muñoz-Rojas[2,*]*

[1] Faculty of Materials Science and Engineering, Phenikaa University, Hanoi 12116, Vietnam
[2] Univ. Grenoble Alpes, CNRS, Grenoble INP, LMGP, Grenoble, France
[3] AlmaScience Colab, Madan Parque, 2829-516 Caparica, Portugal
[4] Department of Mechanical and Mechatronics Engineering, University of Waterloo, Canada

Corresponding authors: huong.nguyenviet@phenikaa-uni.edu.vn; david.munoz-rojas@grenoble-inp.fr

Abstract

Due to its unique optical, electrical, and chemical properties, tin dioxide (SnO_2) thin films attract enormous attention as a potential material for gas sensors, catalysis, low-emissivity coatings for smart windows, transparent electrodes for low-cost solar cells, etc. However, the low-cost and high-throughput fabrication of SnO_2 thin films without producing corrosive or toxic by-products remains challenging. One appealing deposition technique, particularly well-adapted to films presenting nanometric thickness is atomic layer deposition (ALD). In this work, several metalorganic tin-based complexes, namely, tin(IV) tert-butoxide, bis[bis(trimethylsilyl) amino]tin(II), dibutyltin diacetate, tin(II) acetylacetonate, tetrakis(dimethylamino)tin(IV), and dibutyltin bis(acetylacetonate), were explored thanks to DFT calculations. Our theoretical calculations suggest that the three last precursors are very appealing for ALD of SnO_2 thin films. The potential use of these precursors for atmospheric-pressure spatial atomic layer deposition (AP-SALD) is also discussed. For the first time, we experimentally demonstrate the AP-SALD growth of SnO_2 thin films using tin(II) acetylacetonate ($Sn(acac)_2$) and water. We observe that $Sn(acac)_2$ exhibits efficient ALD activity with a relatively large ALD temperature window (140-200 °C), resulting in a growth rate of 0.85±0.03 Å/cyc. XPS analyses show a single Sn $3d_{5/2}$ characteristic peak for Sn^{4+} at 486.8±0.3 eV, indicating that a pure SnO_2 phase is obtained within the ALD temperature window. The as-deposited SnO_2 thin films are in all cases amorphous, and film conductivity increases with the deposition temperature. Hall effect measurements confirm the n-type nature of SnO_2 with a free electron density of about 8×10^{19} cm^{-3}, electron mobility up to 11.2 $cm^2V^{-1}s^{-1,}$ and resistivity of 7×10^{-3} Ωcm for samples deposited at 270 °C.

Keywords: spatial ALD (SALD), atmospheric pressure, Tin(II) acetylacetonate, $Sn(acac)_2$, SnO_2, transparent conductive oxides (TCO)

1. Introduction

Tin dioxide (SnO_2) is a high-bandgap material with several interesting properties, such as excellent electrical conductivity, thermal and chemical stability, earth abundance, and non-toxicity. As a result, SnO_2 is an essential semiconductive oxide in many modern applications including solar cells,[1,2] Li-ion batteries[3], thin-film transistors,[4] gas-diffusion barriers,[5] gas sensors,[6] or transparent electrodes for displays or smart windows.[7] Successful integration of SnO_2 thin films into devices demands strict control of film thickness, uniformity and conformity, and transport properties. Different approaches such as spin-coating,[8] ultrasonic spray pyrolysis,[9] sputtering,[10] chemical vapor deposition (CVD),[11] or atomic layer deposition (ALD)[4,5,12] have been used to deposit SnO_2 thin films. The latter can broaden the applications of SnO_2 thin films due to its unique advantages. Indeed, ALD has been considered as one of the best thin-film growth technologies thanks to its capability of depositing pinhole-free, conformal films at relatively low temperatures.[13–15] Over the past decades, research advances have expanded the use of this surface-controlled layer-by-layer technology for not only microelectronic applications[4,16] but also for the development of biosensors,[17] protective coatings,[18–22] and energy conversion, and storage.[23–30] However, being a vacuum-based technology, ALD's main drawback is a slow growth rate, which is attributed to the slow purging process, alternatingly performed between different precursor injections.[31] Additionally, the use of a vacuum chamber makes conventional ALD technology more difficult and expensive to scale up towards an industrial level. In this context, a variation of the ALD technique, namely atmospheric-pressure spatial ALD (AP-SALD), has been recently attracting much attention since it provides a very fast deposition rate and in a scalable fashion while keeping the unique assets of ALD technology.[32–36] In particular, the AP-SALD approach based on a close-proximity injection head is particularly interesting since it can be readily adapted to the sample size (even allowing area-selective deposition or patterning) and the required process conditions for different precursors or applications.[37] In this work, a customized AP-SALD head was designed and optimized with COMSOL Multiphysics simulation, then fabricated with metal 3D printing technology.[37]

As ALD technology is based on surface reactions between precursor molecules and functional groups on the solid surface, it relies on successful precursor chemistry. The essential requirements for ALD precursors include high volatility, high reactivity, no self-decomposition, and no etching of the growing film.[38] For the ALD of SnO_2 films, inorganic tin precursors such as $SnCl_4$ or SnI_4 have been extensively used. Indeed, the first ALD growth of SnO_2 was performed with $SnCl_4$ and water by Viirola and Niinistö,[39] which was then followed by several other works.[40] However, the high deposition temperatures (300 – 600 °C), low growth rate (~ 0.6 Å/cycle), and issues related to corrosive by-products, i.e. HCl, make these inorganic precursors less attractive for widespread applications. For this reason, the search for tin metalorganic precursors for ALD of SnO_2 thin films has recently attracted much attention from different research groups. There are about 15 types of tin metalorganic precursors successfully used for ALD of SnO_2 thin films, such as tetraallyltin,[12] bis(N-ethoxy-2,2-dimethyl propanamido)tin,[41] tin(IV) t-butoxide,[3] tetrakis(dimethylamino)propyl tin(IV)[4], or tetrakis(dimethylamino) tin(IV).[42,43] But according to our best knowledge, only the latter was studied and successfully used in AP-SALD.[5] Moreover, many co-reactants such as H_2O, H_2O_2, O_3, oxygen plasma, or CH_3COOH were combined with the aforementioned tin metalorganic

precursors. However, tetrakis(dimethylamino) tin(IV) was solely reported to efficiently react with water to form SnO_2 thin films, in both low-pressure ALD[44–46] and atmospheric-pressure SALD processes.[43] Therefore, to advance the field of AP-SALD of SnO_2 thin films, a more in-depth study of the effect of precursor chemistry on the film growth at atmospheric pressure should be carried out.

In this work, we studied various types of precursors for atmospheric ALD of SnO_2, such as alkoxides, β-diketonates, alkylamides, and alkylsilylamides. We first performed DFT calculations to understand their reactivity and evaluate their characteristics and effect on the ALD growth of SnO_2 at different deposition conditions. Three precursors, including tin(II) acetylacetonate, tetrakis(dimethylamino)tin(IV), and dibutyltin bis(acetylacetonate), were identified to be appealing for atmospheric-pressure ALD of SnO_2. In the second stage, we experimentally tested tin(II) acetylacetonate and bis[bis(trimethylsilyl)amino]tin(II) with water as the co-reactant and successfully demonstrated the AP-SALD growth of SnO_2 thin films with tin(II) acetylacetonate. The effect of deposition temperature and pressure on the film growth rate and properties will be presented and discussed. Finally, characterizations of the deposited SnO_2 thin films using X-ray photoelectron spectroscopy (XPS), X-ray diffraction (XRD), and Hall-effect measurement techniques are presented.

2. Experimental and simulation sections

Bond dissociation energy (BDE) was calculated by density functional theory (DFT) using plane-wave basis sets and projector-augmented-wave (PAW) pseudopotentials implemented in the Vienna Ab initio Simulation Package (VASP) version 5.4.4.[47,48] The exchange and correlation term was approximated based on the generalized gradient approximation (GGA) using the Perdew−Burke−Ernzerhof (PBE) functional.[49,50] The isolated precursors were optimized in the gas-phase within large cubic supercells with a dimension of 30 Å using the Γ point sampling for the Brillouin zone integrations and a plane-wave cutoff of 450 eV. The stable structures were optimized until the energy deviation between two consecutive electronic steps was less than 10^{-4} eV. The BDE was calculated by the energy difference between the fully optimized precursor and the fragments produced by the bond-breaking: $\Delta E = E_{fragments} - E_{precursor}$. To minimize the interaction among the separated fragments, the distance between two fragments was set larger than 10 Å. The final BDE value was obtained by averaging the BDE of the same type within a precursor. The molecular structures of different precursors obtained from the DFT optimization were visualized by SAMSON connect software.[51]

SnO_2 thin film depositions were performed in a home-built AP-SALD system equipped with a close-proximity gas injection head. The latter was fabricated with metal 3D printing technology.[37] The head was thoroughly studied with COMSOL Multiphysics Simulation to validate its suitability for our AP-SALD system (see further details in the SI). Bis[bis(trimethylsilyl)amino]tin(II) and tin(II) acetylacetonate ($Sn(acac)_2$) from Sigma-Aldrich were used as tin precursors, while water vapor was employed as the co-reactant. The temperatures of the precursor bubbler and precursor gas lines were maintained at 85 °C and 90 °C, respectively. Metal precursor (one channel), co-reactant (2 channels), and inert purging gas (N_2, 4 channels) were injected onto the substrate surface via the close-proximity gas injection head. The head was placed at 150 μm from the

substrate, which was oscillated underneath at a speed of 2.8 cm/s. The tin precursor was delivered to the substrate by bubbling a N_2 flow through the liquid precursor (150 sccm), which was then diluted with an extra N_2 flow (100 sccm). Similarly, the values used for carrying water vapor to the substrate surface were 200 sccm, both for bubbling and dilution flows. The nitrogen flow in each purging channel was kept at 200 sccm. The borosilicate glass substrates were cleaned using ethanol, deionized water, and then dried under pure nitrogen.

The chemical composition of the deposited films and the oxidation state of Sn were analyzed by XPS. The XPS measurements were performed using a Theta 300 spectrometer, from Thermo Scientific, with an Al $K_{\alpha 1,2}$ (1486.6 eV) X-ray source in ultra-high vacuum conditions of 10^{-9} mbar. The surface of the samples was analyzed without any ion-sputtering cleaning process. The core levels of the Sn and O in the film were probed in the Sn 3d and O 1s energy ranges. The experimental data were fitted with the Advantage software from Thermo Fisher Scientific. The energy scale was calibrated with the C 1s line from carbon contamination at 284.8 eV. The film thickness and optical properties were studied with ellipsometry (Film Sense FS-1) and a PerkinElmer Lambda 950 spectrophotometer in the range of 250−2500 nm. Surface morphology was analyzed with both field-emission-gun scanning electron microscopy (FEG-SEM, Environmental FEI Quanta 250) and atomic force microscopy (AFM, JPK NanoWizard® 4 XP). Atomic structure and crystallinity were studied by XRD (Bruker D8 Advance) in Bragg−Brentano configuration, using 0.15406 nm Cu K_α radiation. The 2θ step and measurement duration for each step were 0.011° and 2 s, respectively. Grazing incidence XRD acquisitions were collected on a RIGAKU Smartlab system. The set-up is equipped with a 9 kW rotating anode Cu source (45 kV and 200 mA). Hall mobility and carrier concentration of SnO_2 thin films were analyzed using a home-built Hall effect analyzer with a magnetic field strength of 0.5 T.

3. Results and discussion

3.1. Precursor selection

To explore the effect of precursor chemistry on the atmospheric ALD of SnO_2 thin films, we studied 6 tin precursors, namely, tetrakis(dimethylamino)tin(IV), tin(IV) tert-butoxide, dibutyltin diacetate, tin(II) acetylacetonate, bis[bis(trimethylsilyl)amino]tin(II), dibutyltin bis(acetylacetonate), named from P1 to P6, respectively. Figure 1 illustrates their molecular structures. These precursors belong to the most important volatile metal complex types, i.e. alkoxides, *β*-diketonates, alkylamides, and alkylsilylamides. As a rule of thumb, the precursor reactivity is related to the dissociation energies of the X–Sn bonds in the molecules (X representing the atom/s coordinating Sn in the different precursors). Table 1 summarizes a few characteristics of the precursors such as melting/boiling point, precursor size, molar mass, and dissociation energy of critical X–Sn bonds. The precursor structures and dissociation energies were obtained using DFT calculations. So far, one of the most successful metalorganic precursors for atmospheric-pressure ALD of tin oxide is tetrakis(dimethylamino)tin(IV) (P1), which has the lowest dissociation energy for the Sn–N bond (166.97 kJ/mol). Additionally, its molecular size, molar mass, and boiling points are also the lowest among others. Because of the steric effect associated with the $–N(CH_3)_3$ ligands, P1 has a weak intermolecular interaction, leading to high volatility.

The growth rate of SnO_2 films depends on the co-reactant. Considering the case of tetrakis(dimethylamino)tin(IV), Mai *et al.* obtained a growth rate of about 0.27 Å/cyc using O_2

plasma at a deposition temperature of 200 °C,[4] while *Elam et al.* obtained growth rates of 1.3, 0.89, and 0.61 Å/cyc using H_2O_2, O_3, and H_2O at 175 °C, respectively.[42] Tanskanen and Bent have investigated the ALD growth characteristics of SnO_2 from P1 and H_2O using DFT and second-order Møller−Plesset perturbation theory calculations.[52] They suggest that the experimentally observed increase in GPC of SnO_x at low temperatures (~100 °C) can be associated with the important role of physisorbed H_2O.[52] Additionally, the growth rate significantly increases with the deposition pressure. Hoffmann *et al.* demonstrated a growth rate of 1.5 Å/cyc with solely H_2O as the co-reactant.[43] However, it is not fully clear if this growth rate was obtained within the pure ALD mode or there is a contribution of the CVD growth mode via an unwanted mixture in the gas phase of precursors and co-reactants. Actually, in AP-SALD technology, the distance between the substrate and the gas injection head is a very critical parameter, which can be slightly increased to facilitate the crosstalk of precursors in the gas phase. This results in thin-film growth via spatial chemical vapor deposition (SCVD) mode.[53–55] While the SCVD mode is promising to deposit films with a remarkably higher deposition rate compared to SALD,[54] it is generally rather complicated to distinguish between the pure SALD mode and the SALD-SCVD mixed mode because both can provide very uniform, conformal coatings.[55] Therefore, the ALD temperature window should be thoroughly determined to ensure SALD growth.

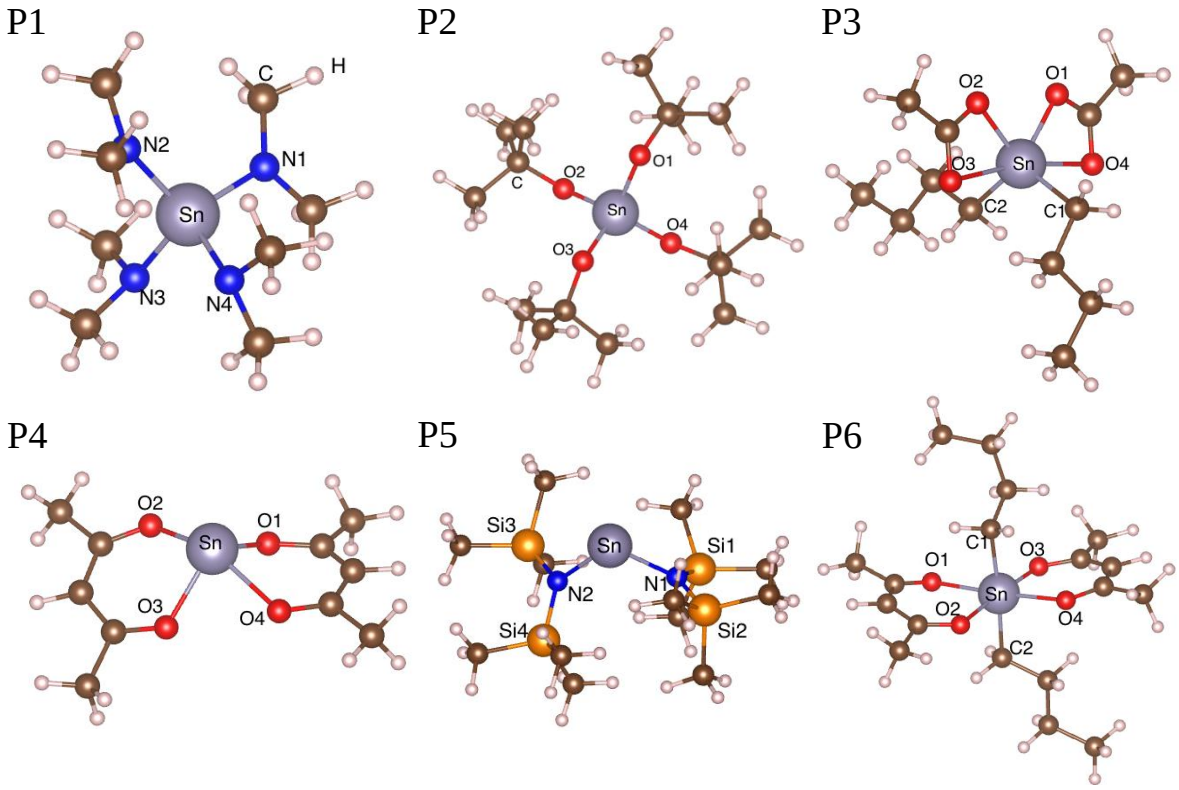

Figure 1: Molecular structures of tin precursors considered in this work, obtained from DFT simulations. From P1 to P6: tetrakis(dimethylamino)tin(IV), tin(IV) tert-butoxide, dibutyltin diacetate, tin(II) acetylacetonate, bis[bis(trimethylsilyl)amino]tin(II), dibutyltin bis(acetylacetonate). Further details related to geometrical parameters of precursor molecules are given in the part I of the SI.

For oxide deposition, alkoxides-based precursors such as tin(IV) tert-butoxide (P2) appear appealing as well. The low boiling temperature, i.e. 65 °C, is originated from its molecular structure

that is surrounded by 12 methyl groups. Our DFT calculation shows that the Sn-O dissociation energy in P2 is remarkably higher than the Sn-N one in P1 (267.27 compared to 166.97 kJ/mol). A few articles showed that the SnO_2 deposition using P2 could be performed with O_2 plasma[3] or CH_3COOH,[56] resulting in amorphous or nanocrystalline phases, respectively. In both cases, a growth rate of about 1 Å/cyc was observed at relatively low temperatures (< 200 °C). At higher deposition temperature, the precursor decomposition cannot be neglected, as stated by Marichy *et al.*[57] Heteroleptic complexes that contain two different ligands, for instance, butyl and acetate as in the case of dibutyltin diacetate (P3), could provide a good compromise between volatility, reactivity, and thermal stability. Several conformers of P3 have been optimized by DFT calculations as demonstrated by Renault et al.[58] Among them, three conformers having two terminal oxygen atoms pointing toward the metal atom are the lowest energy ones. In this work, we also performed DFT optimization and obtained similar results, i.e. the lowest energy conformer (structure 3 of P3 shown in Figure S1) has four oxygen atoms interacting with the Sn atom, making two short Sn-O bonds (2.14 Å) and two long Sn-O bonds (2.58 and 2.60 Å). The Sn-O-C-O dihedral angles are almost zero (0.32° and 1.22°). The dissociation energies for Sn-O and Sn-C are 157.19 kJ/mol and 212.70 kJ/mol, respectively, as indicated in Table 1. Experimentally, Kim *et al.*[59] and Chang *et al.*[60] obtained SnO_2 films with P3 and O_2 plasma, using a deposition temperature of 300 °C. ~~This relatively high deposition temperature required for ALD of SnO_2 could be explained by a high Sn–O dissociation energy (278.85 kJ/mol), as indicated in Table 1~~.

The precursor P4, tin(II) acetyleacetonate, appears to be a very promising precursor due to its low Sn–O dissociation energy (177.54 kJ/mol), which may promote fast half-reactions at the substrate surface and a higher growth rate. Its pure Sn–O bonds (not mixed with Sn–N) may also be beneficial for maximizing the purity of the deposited SnO_x oxides. For instance, Hoffmann *et al.* have observed that the N contamination in SnO_x could increase up to 12% if strong oxidizer such as Ar/O_2 plasma is used in combination with Sn-N -based precursors.[5] Additionally, the P4 precursor has the β-diketonate-type ligand, which usually provides high stability and modest price. The higher thermal stability of P4 (compared to, for instance, metal alkoxides such as P2) originates from the ability to create a metal bond through both oxygen atoms and delocalize the charge of the ligand in the formed C_3O_2M chelate ring (see Figure 1, P4). Indeed, this feature gives tin(II) acetyleacetonate its unique characteristics, i.e., solubility in organic solvents, sufficiently high volatility, and exceptional stability among metalorganic compounds. Previously, tin(II) acetylacetonate was reported in conventional ALD of SnO_x by Selvaraj *et al.*(2014),[61] or ALD of $SnTiO_x$ by Chang *et al.* (2016).[62] In some other works, it was employed in combination with H_2S to deposit SnS,[63–65] or for atomic layer etching of Al_2O_3 using sequential, self-limiting thermal reactions (with HF).[66,67] But it has never been used for atmospheric-pressure ALD of SnO_2 thin films. The experimental study of this precursor for SnO_2 deposition using AP-SALD is presented in detail in the next section.

Precursor P5, bis[bis(trimethylsilyl)amino] tin(II), has a higher Sn–N dissociation energy (295.25 kJ.mol), which would lead to a slower growth rate. Indeed, this precursor has been previously used for ALD of SnO_x using ozone and water,[68] resulting in growth rates of 0.05 – 0.11 Å/cyc (at 80 – 200 °C) and 0.05 – 0.18 Å/cyc (at 100 – 250 °C), respectively. These small values agree with our DFT calculation. This precursor is rather attractive for ALD of SnO_2 because of its

low-cost (see part 2 of the SI). Finally, dibutyltin bis(acetylacetonate), P6, could be a novel potential candidate for atmospheric-pressure ALD of SnO_2. According to our best knowledge, it has never been used in any ALD process. The DFT calculation shown in Table 1 indicates low dissociation energies for Sn–O and Sn–C bonds, i.e. 184.29 and 169.82 kJ/mol, respectively. The Sn atom in the P6 molecule exhibits sp^3d^2 hybrid orbitals, forming an octahedral bonding configuration as illustrated in Figure 1. The fragile Sn–C bonds can be easily broken, resulting in butane gas as a by-product, which can be then purged away with nitrogen. Consequently, the ALD reactivity of P6 is expected to be similar to that of P4 at atmospheric pressure.

Table 1: Melting/boiling temperatures and dissociation energy of critical bonds of 6 types of tin precursors. The temperatures and dissociation energy are obtained from a commercial supplier and our DFT calculation, respectively. The size of precursor molecules are estimated from their optimized structure after DFT calculation

Prec.	Name	Molecular formula	Melting/boiling temperatures	Precursor size (Å)	Molar mass (g/mol)	Bond	Dissociation energy (kJ/mol)
P1	Tetrakis (dimethylamino)tin(IV)	$C_8H_{24}N_4Sn$	n/a / 55 °C	7.4	295.01	Sn—N	166.97
P2	Tin(IV) tert-butoxide	$C_{16}H_{36}O_4Sn$	40 °C / 65 °C	9.1	410.71	Sn—O	267.27
P3	Dibutyltin diacetate	$C_{12}H_{24}O_4Sn$	10 °C / 142 °C	11	350.71	Sn—O	157.19
						Sn—C	212.70
P4	Tin(II) acetylacetonate	$C_{10}H_{14}O_4Sn$	-19 °C / 110 °C	9.7	316.71	Sn—O	177.54
P5	Bis[bis(trimethylsilyl) amino]tin(II)	$C_{12}H_{36}N_2Si_4Sn$	38 °C / 112 °C	11.2	439.05	Sn—N	295.25
						Si—N	408.14
P6	Dibutyltin bis(acetylacetonate)	$C_{18}H_{32}O_4Sn$	26 °C / 150 °C	12.7	430.71	Sn—O	184.29
						Sn—C	169.82

After thoroughly analyzing several criteria, including the volatility, toxicity, as well as precursor cost (see part 2 of the SI), we identified three potential precursors for atmospheric-pressure ALD growth of SnO_2 films, including bis[bis(trimethylsilyl) amino] tin(II), tin(II) acetylacetonate and dibutyltin bis(acetylacetonate). These precursors have, to the best of our knowledge, never been tested for atmospheric-pressure ALD previously. The last precursor is indeed very promising for the AP-SALD process but should be handled with precaution as it and related by-products can be rather toxic. For the discussed reason, we have selected to study the two first precursors using our AP-SALD system. The experimental results will be presented in the following section.

3.2. AP-SALD of SnO_2

The use of bis[bis(trimethylsilyl) amino] tin(II) for AP-SALD results in no film growth with different co-reactants for temperatures ranging from room temperature to 260 °C. We observed that after the first exposure of bis[bis(trimethylsilyl)amino] tin(II) to the surface of the substrate, the substrate appears hydrophobic, thus hindering the film growth whether the subsequent half-reaction uses H_2O, H_2O_2, or O_3 (further details can be found in part 5 of the SI). The hydrophobicity of the substrate surface was previously explained by Crowe & Tolbert,[69] and Tupala *et al.*[68] Indeed, the gaseous by-product of the first half-reaction is bis(trimethylsilyl)amine, also called hexamethyldisilazane (HMDS), which is, in turn, able to react with active sites on the surface to form bulky hydrophobic groups, i.e. $–Si(CH_3)_3$. It should be noted that in the case of conventional low-pressure ALD, the gases have a relatively long mean free path (on the order of mm), therefore, can be removed away from the reaction chamber via the purging step before they can react with

the surface functional groups. In contrast, the mean free path at atmospheric pressure is on the order of a few tens of nm. Therefore, the HMDS molecules have a greater probability of interacting with the surface to create O–Si$(CH_3)_3$ bonds and hinder the growth than in the case of low-pressure ALD. Detailed discussions related to the effect of the deposition pressure on the mean free path of precursors and gaseous by-products, as well as on the gas impingement flux are presented in part 4 of the SI. These results thus show that the working pressure has an important role in the chemistry taking place during the deposition process and has to be taken into account when designing new precursors and processes for AP-SALD.

On the contrary, tin(II) acetylacetonate allows the growth of SnO_2 thin films with AP-SALD. As stated previously, AP-SALD relies on the sequential exposures of precursor and co-reactant to the substrate surface thanks to a gas injection head.[34,70] For each reactant, the volatile molecules are transported from the bubbler to the head via a bubbling flow and a dilution flow, using nitrogen as carrier gas (as presented in Figure 2a). One of the key success factors for the AP-SALD process is the geometrical design of the head.[37] The metalorganic precursor and co-reactant gas flows should be properly distributed to the substrate surface at different locations, as is the case for the head used in this study, as shown in Figure 2b, where the output of a simulation performed using COMSOL Multiphysics software is shown (see also part 3 of the SI). The head was fabricated with metal 3D printing technology.[37] The inset in Figure 2c shows a photograph of an as-deposited SnO_2 film, which was deposited at 200 °C, on a borosilicate glass substrate. The film appears transparent with a yellowish color (film thickness ~ 50 nm). Further details related to the optical properties of SnO_2 films are presented in Figure S7 and S8 of the SI. SEM and AFM micrographs of the as-deposited SnO_2 thin films, shown in Figure 2c-d, indicate a relatively smooth morphology (roughness ~ 4% of the film thickness). The surface morphology of the as-deposited thin films appears granular, despite being amorphous, as shown by the GIXRD diffractograms (Figure 2e). The crystalline phase only appears after annealing at 400 °C or higher for 6 hours. It should be noted that the crystallinity of deposited SnO_2 thin films also depends on the substrate. Part 6 of the SI shows that a film deposited on a silicon wafer is slightly crystallized with the preferential growth orientation (101), while the film deposited on a borosilicate glass substrate with the same experimental conditions is amorphous, even after annealing at 300 °C under vacuum.

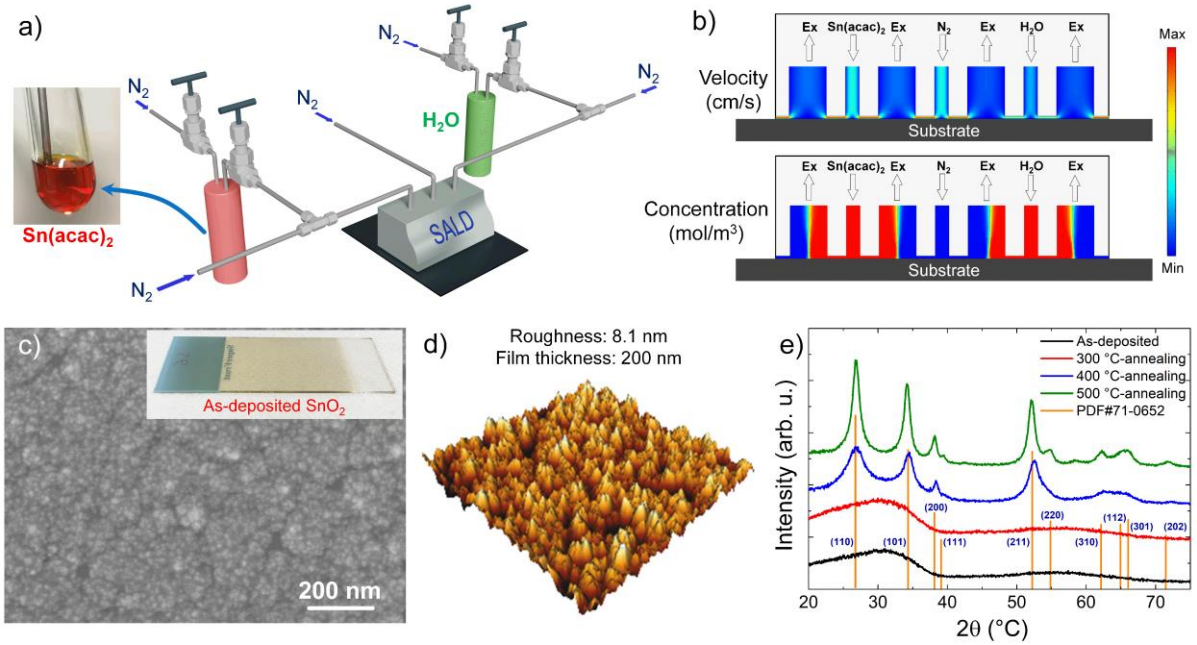

Figure 2: a) schematic illustration of the AP-SALD set-up used for SnO_2 deposition: $Sn(acac)_2$ and water vapor are carried to the gas injection head by inert gas flows (N_2); b) cross-section images of the SALD injection head obtained with COMSOL simulation, showing the distributions of gas velocity and precursor concentration above the substrate surface. The color bar schematically represents values of velocity and precursor concentration, where the hotter color corresponds to higher values; c) top-view SEM micrograph. The inset shows a picture of a 50 nm-thick as-deposited amorphous SnO_2 film on a glass substrate; d) AFM image of a 200 nm-thick SnO_2 film deposited at 200 °C (the scanned area is 2.4μm×2.4μm), and e) grazing incidence XRD of as-deposited (@200 °C) and annealed SnO_2 films on glass.

It is important to note that this is the first time, to the best of our knowledge, that $Sn(acac)_2$ has been successfully used for atmospheric-pressure ALD of SnO_2. So far, the only work reporting the use of $Sn(acac)_2$ for ALD of SnO_2 was done by Selvaraj *et al.*[61] in which they demonstrated a film growth rate of about 1 Å/cycle obtained within the ALD temperature window of 175–300 °C using ozone. Surprisingly, the authors reported that no film growth was observed with water or oxygen as co-reactant. This is in contrast to the experimental results we observed in atmospheric-pressure SALD, i.e. $Sn(acac)_2$ does efficiently react with water at temperatures as low as 120 °C. Figure 3 shows the growth rate and the refractive index of SnO_2 thin films deposited on a glass substrate as a function of deposition temperature. The ALD temperature window appears in a relatively large range of 140 - 200 °C. The growth rate within the ALD window is 0.85±0.03 Å/cyc. As a comparison, using tetrakis(dimethylamino)tin(IV) and H_2O in atmospheric-pressure ALD resulted in a relatively high growth rate, i.e. 1.5 Å/cyc, as reported by Hoffmann *et al.*[43] Recently, Won *et al.* demonstrated that plasma-enhanced ALD (PEALD) of SnO_2 using tetrakis(dimethylamino)tin(IV) and H_2O plasma could even result in a higher growth rate, i.e. ~2.1 Å/cyc, within the temperature range of 100 - 300 °C.[71] Our results show that for the deposition temperature beyond 200 °C, the growth rate increases very quickly, reaching 1 Å/cyc at 260 °C. It is expected that at the higher temperatures, the increased film growth may arise from the self-decomposition of $Sn(acac)_2$ due to the low dissociation energy of Sn-O bonds in the precursor molecule. Because of the very small distance (150 µm) between the hot substrate surface and the injection head made of metal, the latter is also heated (i.e. the head is not thermalized) and could transfer the thermal energy to the precursor-containing gas flows. The self-decomposition of

$Sn(acac)_2$ thus becomes more detrimental at high temperatures (> 200 °C). This phenomenon could affect the purity of the deposited thin films, as corroborated by XPS in the next section, as well as their uniformity and conformality over high-aspect-ratio features. Therefore, for applications that do not present constraints related to conformality or temperature, the fast growth and enhanced electrical properties (discussed later in this section) at high deposition temperature could prove beneficial. Moreover, fast growth in the CVD mode can result in low-refractive index materials,[70] which can be attributed to low film density with porous nanostructured films, or light element contamination (carbon, hydrogen, etc). A similar phenomenon was also observed in PEALD of SnO_2 using tetrakis(dimethylamino)tin(IV) and H_2O plasma, resulting in a refractive index of 1.9–2.0.[71] The authors have also demonstrated that the refractive index slightly decreases for deposition temperatures higher than 200 °C, as being observed in our case.

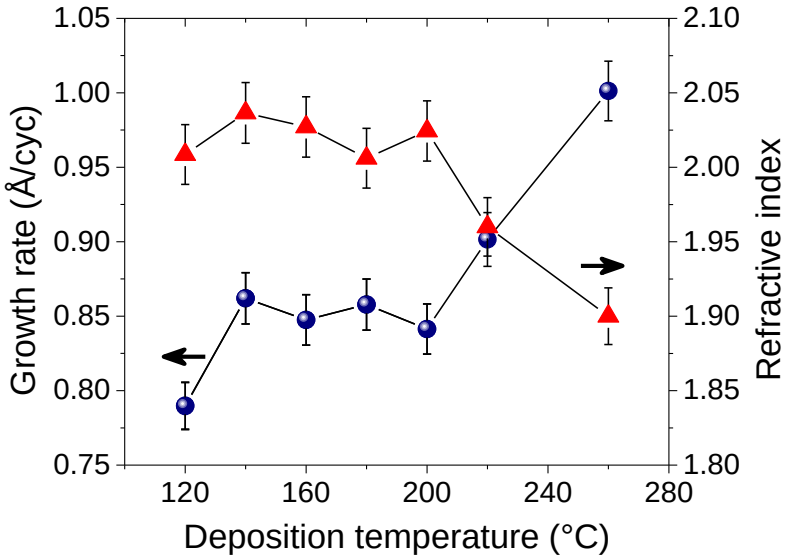

Figure 3: Growth rate and refractive index (@633 nm) of SnO_2 films deposited at various deposition temperatures. The ALD window is observed in the range [140, 200 °C]

The chemical composition and chemical state of Sn and O in the SnO_2 thin films were studied with XPS for a series of films deposited at different temperatures, from 140 °C to 260 °C. As an example, Figure 4 shows XPS spectra of SnO_2 thin films deposited at 180 °C. The Sn $3d_{3/2}$ peak at 495.3 eV and the Sn $3d_{5/2}$ peak at 486.8 eV, as well as the O 1s peak at 530.7 eV, are assigned to SnO_2.[72] The deconvolution of the O1s peak showed two main components: O–Sn^{4+} and O–C peaks (denoted as O1s A and O1s B, respectively). The latter is assigned to surface adsorbed oxygen species and hydroxyl ions (OH–). For comparison, the binding energies of Sn $3d_{5/2}$ in Sn metal, and SnO phases are at about 485.2 eV, and 486 eV, respectively. These values are not very far from the 486.8 eV position but it can be seen in Figure 4b, that they are not observed in our case. Other XPS spectra of SnO_2 thin films deposited at 140, 220, and 260 °C are presented in part 7 of the SI. In all cases, the only phase obtained is SnO_2, which is quite counter-intuitive regarding the Sn^{2+} oxidation state of tin in the original precursor $Sn(acac)_2$ and relatively weak oxidizing power of water vapor. The proposed explanation is that SALD of SnO_2 films was carried out in open-air conditions with a high oxygen content, that apparently plays an important role in the oxidation of Sn^{2+} to Sn^{4+}.

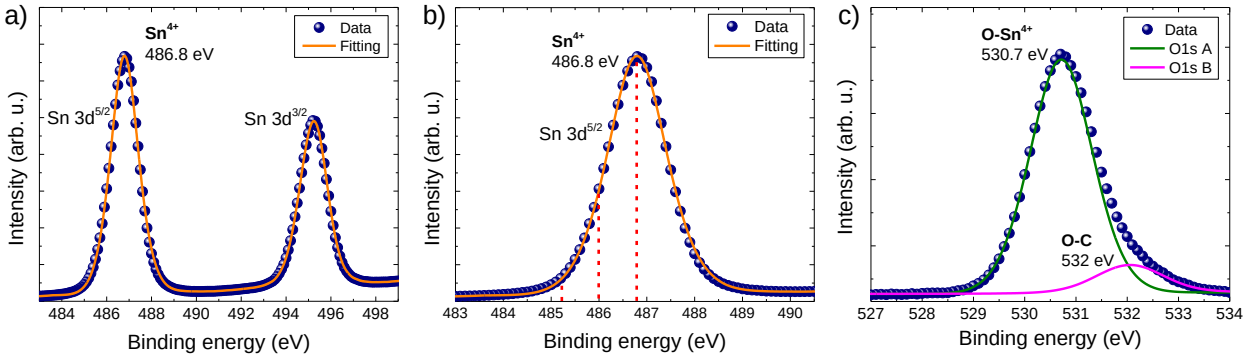

Figure 4: XPS spectra of SnO_2 deposited at 180 °C, a) Sn $3d_{5/2}$ and Sn $3d_{3/2}$ peaks; b) zoomed-in view of Sn $3d_{5/2}$ peak showing the presence of only Sn^{4+} in the films. The binding energies of Sn $3d_{5/2}$ in Sn metal, SnO, and SnO_2 are at about 485.2 eV, 486 eV, and 486.6 eV, indicated by the red dashed lines, respectively; c) deconvolution of O1s peak, showing two main components: O-Sn^{4+} and O-C peaks (denoted as O1s A and O1s B, respectively).

Table 2: Summary of some characteristics of XPS peaks (Sn $3d_{5/2}$, O1s A, O1s B) obtained from SnO_2 samples deposited at temperatures from 140 °C to 260 °C. The error for peak position estimation is 0.1 eV, and for atomic concentration is about 0.2%.

Deposition temperature (°C)	**Peak position (eV)**			**Atomic concentration (%)**				**Ratio**	
	Sn $3d_{5/2}$	O1s A	O1s B	Sn $3d_{5/2}$	O1s A	O1s B	C1s	%O1s A /%Sn $3d_{5/2}$	%O1s B in O1s peak
260	487.0	530.7	531.9	34.3	49.0	12.1	4.6	1.43	20%
220	487.1	531.0	532.2	36.9	55.0	6.7	1.5	1.49	11%
180	486.8	530.7	532.0	39.3	52.4	7.1	1.3	1.33	12%
140	486.5	530.4	531.7	34.2	49.8	11.6	4.3	1.46	19%

A summary of XPS results obtained from samples deposited at various temperatures is presented in Table 2. The position of the Sn $3d_{5/2}$ peak is slightly shifted to higher energy when the deposition temperature increases. The percentage of O1s B (contribution from O-C bonds) is about 19% for the sample deposited at low temperature, i.e. 140 °C, which can be attributed to residual organic ligands not being fully removed and stuck on the solid surface. But interestingly, the same ratio rises to 20% for the sample deposited at 260 °C. Indeed, at such a temperature, the thermal self-decomposition of the precursor is not negligible. This is in agreement with the variation of %C observed in Table 2. The ratio between %O and %Sn in the SnO_2 thin films ranges from 1.33 to 1.49, which is still far below the stoichiometric ratio. Hoffmann *et al.* also observed a similar phenomenon for their tin oxide films deposited with atmospheric-pressure SALD using tetrakis(dimethylamino)tin(IV) and water.[5] In general, the oxygen deficiency in the films could originate from two typical point defects: oxygen vacancies (V_O) or tin interstitials (Sn_i). So far, these defects are widely accepted to be the origins of n-type conductivity in SnO_2 thin films. However, while these defects can explain rather well the non-stoichiometric nature of SnO_2, their responsibility for n-type conductivity in SnO_2 thin films remains unclear. Kılıç and Zunger[73] proposed that Sn_i and V_O produce shallow donor levels in the SnO_2 band structure, resulting in n-type conduction in undoped SnO_2. But a few years later, Singh & Van de Walle *et al.* provided the opposite statement, that intrinsic point defects, such as V_O and Sn_i, are unlikely to be the origin of n-type conductivity in SnO_2, which should be explained by unintended incorporation of impurities, in particular, hydrogen.[74] They found that hydrogen can indeed be incorporated on interstitial sites or substitutional oxygen sites in SnO_2. In our case, we believe the oxygen deficiency in our SnO_2

thin films originates from oxygen vacancies, V_O, and the substitutional hydrogen on oxygen sites, H_O. Indeed, the Sn_i defect has too large a formation energy to be present in a considerable amount.[74]

Table 3: Hall effect measurement of SnO_2 samples deposited at 270 °C.

Film thickness (nm)	Sheet resistance (Ω/sq)	Resistivity (Ωcm)	Electron mobility ($cm^2V^{-1}s^{-1}$)	Carrier concentration (cm^{-3})
61.6	2208.9	1.3×10^{-2}	4.0	1.1×10^{20}
123.1	955.8	1.2×10^{-2}	5.7	9.4×10^{19}
321.5	217.0	7.0×10^{-3}	11.2	8.0×10^{19}

The electrical properties of SnO_2 thin films were investigated using Hall effect measurements at room temperature. The film conductivity was observed to increase with the deposition temperature. For samples deposited at low temperatures (≤ 200 °C), the film appears very resistive with a sheet resistance in the range of MΩ. For samples deposited at 220 °C, the sheet resistance decreases to about tens of kΩ for 60 nm-thick films. Increasing the deposition temperature beyond 270 °C results in highly conductive as-deposited amorphous SnO_2 thin films. Table 3 shows the transport properties of several films deposited at 270 °C having different thicknesses. Electron mobility values up to 11 $cm^2/V/s$ can be obtained while the carrier concentration is rather high, ~ 8×10^{19} cm^{-3}, resulting in resistivity of about 7×10^{-3} Ωcm. For comparison, Selvaraj *et al.* have obtained a resistivity of 0.3 Ωcm for a SnO_2 nanofilm deposited at 300 °C by conventional ALD using the same precursors.[61] Hoffmann *et al.* have demonstrated an electrical resistivity of 10^{-2} Ωcm (carrier mobility: 4.7 $cm^2V^{-1}s^{-1}$, carrier density: 2×10^{20} cm^{-3}) for SnO_2 layers deposited with atmospheric-pressure oxygen plasma or ozone in combination with tetrakis(dimethylamino)tin(IV).[5] Further optimization on the deposition conditions such as the gas flows, doping strategy, or post-deposition treatments should be carried out to further increase the film conductivity. Also, it should be noted that despite the amorphous nature of the SnO_2 thin films, a clear dependence of the electron mobility on the film thickness is observed (Table 3). The influence of the film thickness on the mean free path of free electrons in the SnO_2 thin films is excluded. Indeed, the mean free path is about only 0.8–1 nm in this case (estimated from their mobility, and effective mass), which is much smaller than the film thicknesses considered here. Hence, the thickness-mobility dependence of the conductive amorphous SnO_2 thin films is not fully understood and requires a more detailed study. The as-deposited materials can be post-treated via doping with extrinsic elements or annealing to improve the electrical properties for appropriate applications. In any case, the transport properties obtained here are better than those reported previously. Table 4 compares some important features of SnO_2 thin films deposited with various ALD conditions, including deposition processing pressure, temperature, as well as the type of the substrate. Using water as the co-reactant, and at relatively low deposition temperatures and atmospheric pressure, we obtained a remarkably high film conductivity, up to two orders of magnitude higher compared to films obtained in similar conditions.

Table 4: Comparison of processing parameters and SnO_2 film properties deposited with different ALD techniques.

Precursor	**Co-reactant**	**Deposition pressure**	**Substrate**	**Temperature (°C)**	**Growth rate (Å/cyc)**	**Crystallinity**	**Stoichiometry (%O/%Sn)**	**Conductivity $(\Omega cm)^{-1}$**	**Ref.**
P1	O_3	Atmospheric	Silicon, glass	80 – 165	1.5 (100 °C)	-	2.2	-	5
	O_2 plasma				1.1 @150 °C		2.1 – 2.2	10^{-3} – 10^{2}	

	Water				0.7 @150 °C		1.7	2.3×10^{-3}	
P2	Acetic acid	(vacuum)	Silicon	75 – 250	1.1	crystalline	-	-	[56]
	O_2 plasma	(vacuum)	Stainless steel	200	0.95 – 1.0	amorphous	-	-	[3]
P3	O_2 plasma	550 mTorr	Silicon	200 – 400	1.0	crystalline	1.6 – 2.0	-	[75]
	O_2 plasma	240 mTorr	PAN nanofiber	100	0.8	amorphous	-	-	[76]
P4	O_3	40 mTorr	p-type silicon	175 – 300	1.0	amorphous	2.4	1.67 – 3.34	[61]
P5	O_3	10 mbar	Silicon,	80 – 200	0.05 – 0.11	amorphous	2.1 – 2.5	Non-conductive	[68]
	Water		Soda-lime glass	100 – 250	0.05 – 0.18	crystalline	1.5		
P4	***Water***	***Atmospheric***	***Borosilicate glass***	***120 – 260***	***0.82 – 0.88***	***amorphous***	***1.46 – 1.49***	***77 – 143***	***This work***

In summary, among the several explored precursors in literature, only tetrakis (dimethylamino)tin(IV)[43] and tin(II) acetylacetonate (in this work) have been successfully used for the atmospheric-pressure ALD. Hoffmann *et al.* have tested tetrakis (dimethylamino)tin(IV) in both low-pressure and atmospheric-pressure ALD processes. They demonstrated that the growth rates of SnO_x were 1.1 and 1.5 Å/cyc, respectively. The higher growth rate in the case of atmospheric pressure ALD compared to the conventional ALD was indeed commonly observed. For instance, Mousa *et al.* have observed an increase in the growth rate up to 47 % (from 1.7 Å/cyc to 2.5 Å/cyc) for ZnO when the pressure increases from 2 Torr to 760 Torr.[77] This phenomenon can be explained by analyzing two critical parameters at the microscopic scale: mean free path (mfp), and impingement flux of precursors. While higher impingement flux at the atmospheric pressure (given by the number of molecules colliding with the substrate surface per unit of area and time) leads to a higher growth rate, the mean free path of gases decreases at higher pressure. The lower mean free path is not a critical problem for precursor transport because of the flow-driven nature of most atmospheric-pressure ALD techniques, for instance, AP-SALD. In contrast, it can be an issue if the by-products react with the deposited layer. Indeed, at high pressure, the interaction between the gaseous by-products and the solid films is more probable, leading to unwanted phenomena such as etching or passivating effect, as discussed previously for the case of bis[bis(trimethylsilyl)amino] tin(II). Hence, the selection of precursors for atmospheric-pressure ALD should be taken into account the chemistry compatibility between the underneath layer and the ligands. Besides, precursors with small ligands are preferentially used due to their limited steric hindrances (that reduces the growth rate), as well as to increase the impingement flux (that improves the growth rate). While plasma-enhanced ALD becomes a remarkable tool to reduce the deposition temperature and facilitate the use of the flexible polymeric substrate,[55] the contamination related to the plasma process should also be considered if using precursors containing different elements. For instance, the use of oxygen plasma in combination with tetrakis(dimethylamino)tin(IV) could lead to non-negligible nitrogen contamination in the SnO_x films.[5] With these reasons, the tin-organic precursors for AP-SALD should: i) be as small, and light as possible, ii) have low dissociation energy related to the critical bonds, iii) have Sn-O bonds rather than Sn-C or Sn-N if using plasma-enhanced process, iv) be volatile, non-toxic (also by-products), low-cost and safe when handling the precursors. The price of some tin metalorganic precursors used for ALD is presented in Table S2 of the SI, showing that tin(II) acetylacetonate,

dibutyltin diacetate, and dibutyltin bis(acetylacetonate) are very promising for use in atmospheric pressure ALD technology.

4. Conclusions

In this work, DFT calculations were used to explore different organic tin precursors for atmospheric ALD, including tin(IV) tert-butoxide, bis[bis(trimethylsilyl) amino]tin(II), dibutyltin diacetate, tin(II) acetylacetonate, tetrakis(dimethylamino)tin(IV), dibutyltin bis(acetylacetonate). The theoretical calculations show that the latter three molecules are promising for atmospheric-pressure ALD. In this work, we experimentally tested bis[bis(trimethylsilyl) amino]tin(II) and tin(II) acetylacetonate with the AP-SALD technique. Despite the previous success in conventional ALD, the use of bis[bis(trimethylsilyl) amino] tin(II) for AP-SALD results in no film growth with different co-reactants such as H_2O, H_2O_2, or O_3. By-products of the half-reaction between the precursor and the substrate surface are expected to be hydrophobic $Si(CH_3)_3$ groups, which hinder the film growth. This phenomenon becomes more detrimental at atmospheric pressure than in vacuum due to the strong dependence of the mean free path of gaseous by-products on the working pressure. In contrast, we experimentally demonstrated for the first time that tin(II) acetylacetonate exhibits efficient ALD activity at atmospheric pressure with a large ALD temperature window [140, 200 °C]. The obtained growth rate is remarkably high, i.e. 0.85±0.03 Å/cyc. The as-deposited thin films on borosilicate glass substrates appear amorphous and conductive (for deposition temperatures higher than 220 °C). XPS analysis shows evidence for the SnO_2 phase, indicated by a single characteristic peak for Sn^{4+} at 486.8 eV. The as-deposited SnO_2 thin films exhibit n-type conductivity with a free carrier density of about 10^{20} cm^{-3} and mobility up to 11.2 $cm^2V^{-1}s^{-1}$, resulting in resistivity as low as 7×10^{-3} Ωcm. The carrier transport properties of SnO_2 thin films deposited with tin(II) acetylacetonate at atmospheric pressure are very appealing when compared to previous studies using the same precursor or the other studies on ALD of SnO_2.

Acknowledgments

The authors thank the Agence Nationale de Recherche (ANR, France) via the project DESPATCH (No. ANR-16- CE05-0021). The authors acknowledge the Consortium des Moyens Technologiques Communs (CMTC)—Grenoble INP platform—for the characterization equipment. This research is funded by Vietnam National Foundation for Science and Technology Development (NAFOSTED) under grant number 103.02-2019-341. The authors would like to thank professor A. Kiet Tieu for the use of the VASP package and the Australia National Computational Infrastructure (NCI) for computing time on Gadi.

References

(1) Jiang, Q.; Zhang, X.; You, J. SnO_2: A Wonderful Electron Transport Layer for Perovskite Solar Cells. *Small* **2018**, *14* (31), 1801154. https://doi.org/10.1002/smll.201801154.

(2) Jeong, S.; Seo, S.; Park, H.; Shin, H. Atomic Layer Deposition of a SnO_2 Electron-Transporting Layer for Planar Perovskite Solar Cells with a Power Conversion Efficiency of 18.3%. *Chem. Commun.* **2019**, *55* (17), 2433–2436. https://doi.org/10.1039/C8CC09557D.

(3) Aravindan, V.; Jinesh, K. B.; Prabhakar, R. R.; Kale, V. S.; Madhavi, S. Atomic Layer Deposited (ALD) SnO_2 Anodes with Exceptional Cycleability for Li-Ion Batteries. *Nano Energy* **2013**, *2* (5), 720–725. https://doi.org/10.1016/j.nanoen.2012.12.007.

(4) Mai, L.; Zanders, D.; Subaşı, E.; Ciftyurek, E.; Hoppe, C.; Rogalla, D.; Gilbert, W.; Arcos, T. de los; Schierbaum, K.; Grundmeier, G.; Bock, C.; Devi, A. Low-Temperature Plasma-Enhanced Atomic Layer Deposition of Tin(IV) Oxide from a Functionalized Alkyl Precursor: Fabrication and Evaluation of SnO_2-Based Thin-Film Transistor Devices. *ACS Appl. Mater. Interfaces* **2019**, *11* (3), 3169–3180. https://doi.org/10.1021/acsami.8b16443.

(5) Hoffmann, L.; Theirich, D.; Schlamm, D.; Hasselmann, T.; Pack, S.; Brinkmann, K. O.; Rogalla, D.; Peters, S.; Räupke, A.; Gargouri, H.; Riedl, T. Atmospheric Pressure Plasma Enhanced Spatial Atomic Layer Deposition of SnO_x as Conductive Gas Diffusion Barrier. *Journal of Vacuum Science & Technology A* **2018**, *36* (1), 01A112. https://doi.org/10.1116/1.5006781.

(6) Das, S.; Jayaraman, V. SnO_2: A Comprehensive Review on Structures and Gas Sensors. *Progress in Materials Science* **2014**, *66*, 112–255. https://doi.org/10.1016/j.pmatsci.2014.06.003.

(7) Dalapati, G. K.; Sharma, H.; Guchhait, A.; Chakrabarty, N.; Bamola, P.; Liu, Q.; Saianand, G.; Sai Krishna, A. M.; Mukhopadhyay, S.; Dey, A.; Wong, T. K. S.; Zhuk, S.; Ghosh, S.; Chakrabortty, S.; Mahata, C.; Biring, S.; Kumar, A.; Ribeiro, C. S.; Ramakrishna, S.; Chakraborty, A. K.; Krishnamurthy, S.; Sonar, P.; Sharma, M. Tin Oxide for Optoelectronic, Photovoltaic and Energy Storage Devices: A Review. *J. Mater. Chem. A* **2021**, *9* (31), 16621–16684. https://doi.org/10.1039/D1TA01291F.

(8) Han, G. S.; Kim, J.; Bae, S.; Han, S.; Kim, Y. J.; Gong, O. Y.; Lee, P.; Ko, M. J.; Jung, H. S. Spin-Coating Process for 10 Cm × 10 Cm Perovskite Solar Modules Enabled by Self-Assembly of SnO_2 Nanocolloids. *ACS Energy Lett.* **2019**, *4* (8), 1845–1851. https://doi.org/10.1021/acsenergylett.9b00953.

(9) Consonni, V.; Rey, G.; Roussel, H.; Bellet, D. Thickness Effects on the Texture Development of Fluorine-Doped SnO_2 Thin Films: The Role of Surface and Strain Energy. *Journal of Applied Physics* **2012**, *111* (3), 033523. https://doi.org/10.1063/1.3684543.

(10) Kam, M.; Zhang, Q.; Zhang, D.; Fan, Z. Room-Temperature Sputtered SnO_2 as Robust Electron Transport Layer for Air-Stable and Efficient Perovskite Solar Cells on Rigid and Flexible Substrates. *Sci Rep* **2019**, *9* (1), 6963. https://doi.org/10.1038/s41598-019-42962-9.

(11) Lu, Y. M.; Jiang, J.; Becker, M.; Kramm, B.; Chen, L.; Polity, A.; He, Y. B.; Klar, P. J.; Meyer, B. K. Polycrystalline SnO_2 Films Grown by Chemical Vapor Deposition on Quartz Glass. *Vacuum* **2015**, *122*, 347–352. https://doi.org/10.1016/j.vacuum.2015.03.018.

(12) Muneshwar, T.; Barlage, D.; Cadien, K. Tetraallyltin Precursor for Plasma Enhanced Atomic Layer Deposition of Tin Oxide: Growth Study and Material Characterization. *Journal of Vacuum Science & Technology A* **2019**, *37* (3), 030601. https://doi.org/10.1116/1.5091944.

(13) George, S. M. Atomic Layer Deposition: An Overview. *Chemical Reviews* **2010**, *110* (1), 111–131. https://doi.org/10.1021/cr900056b.

(14) Van Bui, H.; Grillo, F.; van Ommen, J. R. Atomic and Molecular Layer Deposition: Off the Beaten Track. *Chemical Communications* **2017**, *53* (1), 45–71. https://doi.org/10.1039/C6CC05568K.

(15) Cremers, V.; Puurunen, R. L.; Dendooven, J. Conformality in Atomic Layer Deposition: Current Status Overview of Analysis and Modelling. *Applied Physics Reviews* **2019**, *6* (2), 021302. https://doi.org/10.1063/1.5060967.

(16) Johnson, R. W.; Hultqvist, A.; Bent, S. F. A Brief Review of Atomic Layer Deposition: From Fundamentals to Applications. *Materials Today* **2014**, *17* (5), 236–246. https://doi.org/10.1016/j.mattod.2014.04.026.

(17) Graniel, O.; Weber, M.; Balme, S.; Miele, P.; Bechelany, M. Atomic Layer Deposition for Biosensing Applications. *Biosensors and Bioelectronics* **2018**, *122*, 147–159. https://doi.org/10.1016/j.bios.2018.09.038.

(18) Park, J.-S.; Chae, H.; Chung, H. K.; Lee, S. I. Thin Film Encapsulation for Flexible AM-OLED: A Review. *Semicond. Sci. Technol.* **2011**, *26* (3), 034001. https://doi.org/10.1088/0268-1242/26/3/034001.

(19) Maindron, T.; Jullien, T.; André, A. Defect Analysis in Low Temperature Atomic Layer Deposited Al_2O_3 and Physical Vapor Deposited SiO Barrier Films and Combination of Both to Achieve High Quality Moisture Barriers. *Journal of Vacuum Science & Technology A: Vacuum, Surfaces, and Films* **2016**, *34* (3), 031513. https://doi.org/10.1116/1.4947289.

(20) Singh, A. K.; Adstedt, K.; Brown, B.; Singh, P. M.; Graham, S. Development of ALD Coatings for Harsh Environment Applications. *ACS Appl. Mater. Interfaces* **2019**, *11* (7), 7498–7509. https://doi.org/10.1021/acsami.8b11557.

(21) Khan, A.; Nguyen, V. H.; Muñoz-Rojas, D.; Aghazadehchors, S.; Jiménez, C.; Nguyen, N. D.; Bellet, D. Stability Enhancement of Silver Nanowire Networks with Conformal ZnO Coatings Deposited by Atmospheric Pressure Spatial Atomic Layer Deposition. *ACS Applied Materials & Interfaces* **2018**, *10* (22), 19208–19217. https://doi.org/10.1021/acsami.8b03079.

(22) Nguyen, V. H.; Resende, J.; Papanastasiou, D. T.; Fontanals, N.; Jiménez, C.; Muñoz-Rojas, D.; Bellet, D. Low-Cost Fabrication of Flexible Transparent Electrodes Based on Al Doped ZnO and Silver Nanowire Nanocomposites: Impact of the Network Density. *Nanoscale* **2019**, *11* (25), 12097–12107. https://doi.org/10.1039/C9NR02664A.

(23) Liu, R.; Lin, Y.; Chou, L.-Y.; Sheehan, S. W.; He, W.; Zhang, F.; Hou, H. J. M.; Wang, D. Water Splitting by Tungsten Oxide Prepared by Atomic Layer Deposition and Decorated with an Oxygen-Evolving Catalyst. *Angewandte Chemie International Edition* **2011**, *50* (2), 499–502. https://doi.org/10.1002/anie.201004801.

(24) Meng, X.; Yang, X.-Q.; Sun, X. Emerging Applications of Atomic Layer Deposition for Lithium-Ion Battery Studies. *Advanced Materials* **2012**, *24* (27), 3589–3615. https://doi.org/10.1002/adma.201200397.

(25) Bui, H. V.; Grillo, F.; Sharath Kulkarni, S.; Bevaart, R.; Thang, N. V.; Linden, B. van der; A. Moulijn, J.; Makkee, M.; T. Kreutzer, M.; Ommen, J. R. van. Low-Temperature Atomic Layer Deposition Delivers More Active and Stable Pt-Based Catalysts. *Nanoscale* **2017**, *9* (30), 10802–10810. https://doi.org/10.1039/C7NR02984E.

(26) Kim, M.-W.; Kim, K.; Ohm, T. Y.; Yoon, H.; Joshi, B.; Samuel, E.; Swihart, M. T.; Choi, S. K.; Park, H.; Yoon, S. S. Electrosprayed BiVO4 Nanopillars Coated with Atomic-Layer-Deposited ZnO/TiO2 as Highly Efficient Photoanodes for Solar Water Splitting. *Chemical Engineering Journal* **2018**, *333*, 721–729. https://doi.org/10.1016/j.cej.2017.09.130.

(27) Grillo, F.; Van Bui, H.; La Zara, D.; Aarnink, A. A. I.; Kovalgin, A. Y.; Kooyman, P.; Kreutzer, M. T.; van Ommen, J. R. From Single Atoms to Nanoparticles: Autocatalysis and Metal Aggregation in Atomic Layer Deposition of Pt on TiO_2 Nanopowder. *Small* **2018**, *14* (23), 1800765. https://doi.org/10.1002/smll.201800765.

(28) Liu, M.; Xue, F.; Wang, X.; Fu, W.; Wang, Y.; Lu, Y.; Li, N. Conformal Deposition of Atomic TiO2 Layer on Chalcogenide Nanorod with Excellent Activity and Durability towards Solar H2 Generation. *Chemical Engineering Journal* **2018**, *341*, 335–343. https://doi.org/10.1016/j.cej.2018.02.031.

(29) Fang, W.-Z.; Tang, Y.-Q.; Ban, C.; Kang, Q.; Qiao, R.; Tao, W.-Q. Atomic Layer Deposition in Porous Electrodes: A Pore-Scale Modeling Study. *Chemical Engineering Journal* **2019**, *378*, 122099. https://doi.org/10.1016/j.cej.2019.122099.

(30) Zhao, Y.; Zhang, L.; Liu, J.; Adair, K.; Zhao, F.; Sun, Y.; Wu, T.; Bi, X.; Amine, K.; Lu, J.; Sun, X. Atomic/Molecular Layer Deposition for Energy Storage and Conversion. *Chemical Society Reviews* **2021**, *50* (6), 3889–3956. https://doi.org/10.1039/D0CS00156B.

(31) Muñoz-Rojas, D.; Maindron, T.; Esteve, A.; Piallat, F.; Kools, J. C. S.; Decams, J.-M. Speeding up the Unique Assets of Atomic Layer Deposition. *Materials Today Chemistry* **2019**, *12*, 96–120. https://doi.org/10.1016/j.mtchem.2018.11.013.

(32) Illiberi, A.; Roozeboom, F.; Poodt, P. Spatial Atomic Layer Deposition of Zinc Oxide Thin Films. *ACS applied materials & interfaces* **2012**, *4* (1), 268–272. https://doi.org/10.1021/am2013097.

(33) Muñoz-Rojas, D.; MacManus-Driscoll, J. Spatial Atmospheric Atomic Layer Deposition: A New Laboratory and Industrial Tool for Low-Cost Photovoltaics. *Mater. Horiz.* **2014**, *1* (3), 314–320. https://doi.org/10.1039/C3MH00136A.

(34) Muñoz-Rojas, D.; Nguyen, V. H.; Masse de la Huerta, C.; Aghazadehchors, S.; Jiménez, C.; Bellet, D. Spatial Atomic Layer Deposition (SALD), an Emerging Tool for Energy Materials. Application to New-Generation Photovoltaic Devices and Transparent Conductive Materials. *Comptes Rendus Physique* **2017**, *18* (7), 391–400. https://doi.org/10.1016/j.crhy.2017.09.004.

(35) Sekkat, A.; Nguyen, V. H.; Masse de La Huerta, C. A.; Rapenne, L.; Bellet, D.; Kaminski-Cachopo, A.; Chichignoud, G.; Muñoz-Rojas, D. Open-Air Printing of Cu_2O Thin Films with High Hole Mobility for Semitransparent Solar Harvesters. *Commun Mater* **2021**, *2* (1), 1–10. https://doi.org/10.1038/s43246-021-00181-8.

(36) Muñoz-Rojas, D.; Huong Nguyen, V.; Masse de la Huerta, C.; Jiménez, C.; Bellet, D. Spatial Atomic Layer Deposition. In *Chemical Vapor Deposition for Nanotechnology*; Mandracci, P., Ed.; IntechOpen, 2019. https://doi.org/10.5772/intechopen.82439.

(37) Huerta, C. A. M. de la; Nguyen, V. H.; Sekkat, A.; Crivello, C.; Toldra-Reig, F.; Veiga, P. B.; Quessada, S.; Jimenez, C.; Muñoz-Rojas, D. Gas-Phase 3D Printing of Functional Materials. *Advanced Materials Technologies* **2020**, *5* (12), 2000657. https://doi.org/10.1002/admt.202000657.

(38) Leskelä, M.; Niinistö, J.; Ritala, M. Atomic Layer Deposition. In *Comprehensive Materials Processing*; Elsevier, 2014; pp 101–123. https://doi.org/10.1016/B978-0-08-096532-1.00401-5.

(39) Viirola, H.; Niinistö, L. Controlled Growth of Tin Dioxide Thin Films by Atomic Layer Epitaxy. *Thin Solid Films* **1994**, *249* (2), 144–149. https://doi.org/10.1016/0040-6090(94)90752-8.

(40) Nazarov, D. V.; Bobrysheva, N. P.; Osmolovskaya, O. M.; Osmolovsky, M. G.; Smirnov, V. M. Atomic Layer Deposition of Tin Dioxide Nanofilms: A Review. *Reviews on Advanced Materials Science* **2015**, *40*, 262–275.

(41) Kim, H. Y.; Nam, J. H.; George, S. M.; Park, J.-S.; Park, B. K.; Kim, G. H.; Jeon, D. J.; Chung, T.-M.; Han, J. H. Phase-Controlled SnO_2 and SnO Growth by Atomic Layer Deposition Using Bis(N-Ethoxy-2,2-Dimethyl Propanamido)Tin Precursor. *Ceramics International* **2019**, *45* (4), 5124–5132. https://doi.org/10.1016/j.ceramint.2018.09.263.

(42) Elam, J. W.; Baker, D. A.; Hryn, A. J.; Martinson, A. B. F.; Pellin, M. J.; Hupp, J. T. Atomic Layer Deposition of Tin Oxide Films Using Tetrakis(Dimethylamino) Tin. *Journal of Vacuum Science & Technology A* **2008**, *26* (2), 244–252. https://doi.org/10.1116/1.2835087.

(43) Hoffmann, L.; Brinkmann, K. O.; Malerczyk, J.; Rogalla, D.; Becker, T.; Theirich, D.; Shutsko, I.; Görrn, P.; Riedl, T. Spatial Atmospheric Pressure Atomic Layer Deposition of Tin Oxide as an Impermeable Electron Extraction Layer for Perovskite Solar Cells with Enhanced Thermal Stability. *ACS Applied Materials & Interfaces* **2018**, *10* (6), 6006–6013. https://doi.org/10.1021/acsami.7b17701.

(44) Mullings, M. N.; Hägglund, C.; Bent, S. F. Tin Oxide Atomic Layer Deposition from Tetrakis(Dimethylamino)Tin and Water. *Journal of Vacuum Science & Technology A* **2013**, *31* (6), 061503. https://doi.org/10.1116/1.4812717.

(45) Hultqvist, A.; Aitola, K.; Sveinbjörnsson, K.; Saki, Z.; Larsson, F.; Törndahl, T.; Johansson, E.; Boschloo, G.; Edoff, M. Atomic Layer Deposition of Electron Selective SnO_x and ZnO Films on Mixed Halide Perovskite: Compatibility and Performance. *ACS Appl. Mater. Interfaces* **2017**, *9* (35), 29707–29716. https://doi.org/10.1021/acsami.7b07627.

(46) Ramachandran, R. K.; Filez, M.; Dendooven, J.; Galvita, V. V.; Poelman, H.; Solano, E.; Fonda, E.; Marin, G. B.; Detavernier, C. Size- and Composition-Controlled Pt–Sn Bimetallic Nanoparticles Prepared by Atomic Layer Deposition. *RSC Adv.* **2017**, *7* (33), 20201–20205. https://doi.org/10.1039/C7RA01463E.

(47) Kresse, G.; Hafner, J. Ab Initio Molecular-Dynamics Simulation of the Liquid-Metal--Amorphous-Semiconductor Transition in Germanium. *Phys. Rev. B* **1994**, *49* (20), 14251–14269. https://doi.org/10.1103/PhysRevB.49.14251.

(48) Kresse, G.; Furthmüller, J. Efficient Iterative Schemes for Ab Initio Total-Energy Calculations Using a Plane-Wave Basis Set. *Phys. Rev. B* **1996**, *54* (16), 11169–11186. https://doi.org/10.1103/PhysRevB.54.11169.

(49) Perdew, J. P.; Chevary, J. A.; Vosko, S. H.; Jackson, K. A.; Pederson, M. R.; Singh, D. J.; Fiolhais, C. Atoms, Molecules, Solids, and Surfaces: Applications of the Generalized Gradient Approximation for Exchange and Correlation. *Phys. Rev. B* **1992**, *46* (11), 6671–6687. https://doi.org/10.1103/PhysRevB.46.6671.

(50) Perdew, J. P.; Burke, K.; Ernzerhof, M. Generalized Gradient Approximation Made Simple. *Physical Review Letters* **1996**, *77* (18), 3865–3868. https://doi.org/10.1103/PhysRevLett.77.3865.

(51) SAMSON Connect https://www.samson-connect.net/.

(52) Tanskanen, J. T.; Bent, S. F. Insights into the Surface Chemistry of Tin Oxide Atomic Layer Deposition from Quantum Chemical Calculations. *J. Phys. Chem. C* **2013**, *117* (37), 19056–19062. https://doi.org/10.1021/jp4063324.

(53) Musselman, K. P.; Muñoz-Rojas, D.; Hoye, R. L. Z.; Sun, H.; Sahonta, S.-L.; Croft, E.; Böhm, M. L.; Ducati, C.; MacManus-Driscoll, J. L. Rapid Open-Air Deposition of Uniform, Nanoscale, Functional Coatings on Nanorod Arrays. *Nanoscale Horizons* **2017**, *2* (2), 110–117. https://doi.org/10.1039/C6NH00197A.

(54) Masse de la Huerta, C.; Nguyen, V. H.; Dedulle, J.-M.; Bellet, D.; Jiménez, C.; Muñoz-Rojas, D. Influence of the Geometric Parameters on the Deposition Mode in Spatial Atomic Layer Deposition: A Novel Approach to Area-Selective Deposition. *Coatings* **2019**, *9* (1), 5. https://doi.org/10.3390/coatings9010005.

(55) Nguyen, V. H.; Sekkat, A.; Masse de la Huerta, C. A.; Zoubian, F.; Crivello, C.; Rubio-Zuazo, J.; Jaffal, M.; Bonvalot, M.; Vallée, C.; Aubry, O.; Rabat, H.; Hong, D.; Muñoz-Rojas, D. Atmospheric Plasma-Enhanced Spatial Chemical Vapor Deposition of SiO2 Using Trivinylmethoxysilane and Oxygen Plasma. *Chem. Mater.* **2020**, *32* (12), 5153–5161. https://doi.org/10.1021/acs.chemmater.0c01148.

(56) Marichy, C.; Donato, N.; Willinger, M.-G.; Latino, M.; Karpinsky, D.; Yu, S.-H.; Neri, G.; Pinna, N. Tin Dioxide Sensing Layer Grown on Tubular Nanostructures by a Non-Aqueous Atomic Layer Deposition Process. *Adv. Funct. Mater.* **2011**, *21* (4), 658–666. https://doi.org/10.1002/adfm.201001572.

(57) Marichy, C.; Silva, R. M.; Pinna, N.; Willinger, M.-G.; Donato, N.; Neri, G. Non-Aqueous Atomic Layer Deposition of SnO2 for Gas Sensing Application. *ECS Transactions* **2018**.

(58) Renault, B.; Cloutet, E.; Cramail, H.; Hannachi, Y.; Tassaing, T. A Combined Spectroscopic and Theoretical Study of Dibutyltin Diacetate and Dilaurate in Supercritical CO2. *J. Phys. Chem. A* **2008**, *112* (36), 8379–8386. https://doi.org/10.1021/jp8004822.

(59) Kim, S.; Kim, D.-H.; Hong, S.-H. Epitaxial Growth of Orthorhombic SnO2 Films on Various YSZ Substrates by Plasma Enhanced Atomic Layer Deposition. *Journal of Crystal Growth* **2012**, *348* (1), 15–19. https://doi.org/10.1016/j.jcrysgro.2012.03.047.

(60) Chang, I.; Kim, D.; Lee, Y.; Hong, S.-H.; Cha, S. W. Effect of Ultra-Thin SnO2 Coating on Pt Catalyst for Energy Applications. *Int. J. Precis. Eng. Manuf.* **2016**, *17* (5), 691–694. https://doi.org/10.1007/s12541-016-0085-x.

(61) Kannan Selvaraj, S.; Feinerman, A.; Takoudis, C. G. Growth Behavior and Properties of Atomic Layer Deposited Tin Oxide on Silicon from Novel Tin(II)Acetylacetonate Precursor and Ozone. *Journal of Vacuum Science & Technology A: Vacuum, Surfaces, and Films* **2014**, *32* (1), 01A112. https://doi.org/10.1116/1.4837915.

(62) Chang, S.; Selvaraj, S. K.; Choi, Y.-Y.; Hong, S.; Nakhmanson, S. M.; Takoudis, C. G. Atomic Layer Deposition of Environmentally Benign SnTiOx as a Potential Ferroelectric Material. *Journal of Vacuum Science & Technology A: Vacuum, Surfaces, and Films* **2015**, *34* (1), 01A119. https://doi.org/10.1116/1.4935650.

(63) Kim, J. Y.; George, S. M. Tin Monosulfide Thin Films Grown by Atomic Layer Deposition Using Tin 2,4-Pentanedionate and Hydrogen Sulfide. *J. Phys. Chem. C* **2010**, *114* (41), 17597–17603. https://doi.org/10.1021/jp9120244.

(64) Browning, R.; Plachinda, P.; Padigi, P.; Solanki, R.; Rouvimov, S. Growth of Multiple WS_2/SnS Layered Semiconductor Heterojunctions. *Nanoscale* **2016**, *8* (4), 2143–2148. https://doi.org/10.1039/C5NR08006A.

(65) Bilousov, O. V.; Ren, Y.; Törndahl, T.; Donzel-Gargand, O.; Ericson, T.; Platzer-Björkman, C.; Edoff, M.; Hägglund, C. Atomic Layer Deposition of Cubic and Orthorhombic Phase Tin Monosulfide. *Chem. Mater.* **2017**, *29* (7), 2969–2978. https://doi.org/10.1021/acs.chemmater.6b05323.

(66) Lee, Y.; George, S. M. Atomic Layer Etching of Al_2O_3 Using Sequential, Self-Limiting Thermal Reactions with $Sn(Acac)_2$ and Hydrogen Fluoride. *ACS Nano* **2015**, *9* (2), 2061–2070. https://doi.org/10.1021/nn507277f.

(67) Lee, Y.; DuMont, J. W.; George, S. M. Mechanism of Thermal Al_2O_3 Atomic Layer Etching Using Sequential Reactions with $Sn(Acac)_2$ and HF. *Chem. Mater.* **2015**, *27* (10), 3648–3657. https://doi.org/10.1021/acs.chemmater.5b00300.

(68) Tupala, J.; Kemell, M.; Mattinen, M.; Meinander, K.; Seppälä, S.; Hatanpää, T.; Räisänen, J.; Ritala, M.; Leskelä, M. Atomic Layer Deposition of Tin Oxide Thin Films from Bis[Bis(Trimethylsilyl)Amino]Tin(II) with Ozone and Water. *Journal of Vacuum Science & Technology A: Vacuum, Surfaces, and Films* **2017**, *35* (4), 041506. https://doi.org/10.1116/1.4984279.

(69) Crowe, L. L.; Tolbert, L. M. Silica Passivation Efficiency Monitored By a Surface-Bound Fluorescent Dye. *Langmuir* **2008**, *24* (16), 8541–8546. https://doi.org/10.1021/la801343b.

(70) Nguyen, V. H.; Sekkat, A.; Jiménez, C.; Muñoz, D.; Bellet, D.; Muñoz-Rojas, D. Impact of Precursor Exposure on Process Efficiency and Film Properties in Spatial Atomic Layer Deposition. *Chemical Engineering Journal* **2021**, *403*, 126234. https://doi.org/10.1016/j.cej.2020.126234.

(71) Won, J. H.; Han, S. H.; Park, B. K.; Chung, T.-M.; Han, J. H. Effect of Oxygen Source on the Various Properties of SnO_2 Thin Films Deposited by Plasma-Enhanced Atomic Layer Deposition. *Coatings* **2020**, *10* (7), 692. https://doi.org/10.3390/coatings10070692.

(72) Kuang, Y.; Zardetto, V.; van Gils, R.; Karwal, S.; Koushik, D.; Verheijen, M. A.; Black, L. E.; Weijtens, C.; Veenstra, S.; Andriessen, R.; Kessels, W. M. M.; Creatore, M. Low-Temperature Plasma-Assisted Atomic-Layer-Deposited SnO_2 as an Electron Transport Layer in Planar Perovskite Solar Cells. *ACS Appl. Mater. Interfaces* **2018**, *10* (36), 30367–30378. https://doi.org/10.1021/acsami.8b09515.

(73) Kılıç, Ç.; Zunger, A. Origins of Coexistence of Conductivity and Transparency in SnO2. *Phys. Rev. Lett.* **2002**, *88* (9), 095501. https://doi.org/10.1103/PhysRevLett.88.095501.

(74) Singh, A. K.; Janotti, A.; Scheffler, M.; Van de Walle, C. G. Sources of Electrical Conductivity in SnO_2. *Phys. Rev. Lett.* **2008**, *101* (5), 055502. https://doi.org/10.1103/PhysRevLett.101.055502.

(75) Choi, G.; Satyanarayana, L.; Park, J. Effect of Process Parameters on Surface Morphology and Characterization of PE-ALD SnO_2 Thin Films for Gas Sensing. *Applied Surface Science* **2006**, *252* (22), 7878–7883. https://doi.org/10.1016/j.apsusc.2005.09.069.

(76) Kim, W.-S.; Lee, B.-S.; Kim, D.-H.; Kim, H.-C.; Yu, W.-R.; Hong, S.-H. SnO_2 Nanotubes Fabricated Using Electrospinning and Atomic Layer Deposition and Their Gas Sensing Performance. *Nanotechnology* **2010**, *21* (24), 245605. https://doi.org/10.1088/0957-4484/21/24/245605.

(77) Mousa, M. B. M.; Oldham, C. J.; Jur, J. S.; Parsons, G. N. Effect of Temperature and Gas Velocity on Growth per Cycle during Al2O3 and ZnO Atomic Layer Deposition at Atmospheric Pressure. *Journal of Vacuum Science & Technology A: Vacuum, Surfaces, and Films* **2012**, *30* (1), 01A155. https://doi.org/10.1116/1.3670961.